Supplement of Atmos. Chem. Phys., 21, 9089–9104, 2021
https://doi.org/10.5194/acp-21-9089-2021-supplement

Atmospheric Chemistry and Physics
Open Access
EGU

Supplement of

Urban organic aerosol composition in eastern China differs from north to south: molecular insight from a liquid chromatography–mass spectrometry (Orbitrap) study

Kai Wang et al.

Correspondence to: Ru-Jin Huang (rujin.huang@ieecas.cn) and Thorsten Hoffmann (t.hoffmann@uni-mainz.de)

Table S1: The daily average concentrations of $PM_{2.5}$, SO_2, NO_2, CO and O_3, average temperature (T) and daily solar radiation in Changchun, Shanghai and Guangzhou during filter sampling dates

Sample ID	Sampling Date	$PM_{2.5}$ ($\mu g\ m^{-3}$)	SO_2 ($\mu g\ m^{-3}$)	NO_2 ($\mu g\ m^{-3}$)	CO ($mg\ m^{-3}$)	O_3 ($\mu g\ m^{-3}$)	T (°C)	Solar radiation ($J\ cm^{-2}$)
Changchun	04/01/2014	222	72	63	1.5	43	−14	841*
	24/01/2014	162	77	51	1.4	70	−11	485*
	29/01/2014	185	70	29	0.9	58	−9	576*
Shanghai	01/01/2014	171	63	99	1.7	61	10	1133*
	19/01/2014	159	33	61	1.3	74	7	1307
	20/01/2014	172	59	76	1.8	42	6	994
Guangzhou	05/01/2014	152	39	89	1.4	113	16	1372
	06/01/2014	138	42	109	1.7	117	15	1164
	11/01/2014	138	24	80	1.6	69	16	1329

The data of SO_2, NO_2, CO, O_3 and T have been taken from an open air quality database (www.aqistudy.cn), while the data of solar radiation wereprovided by the World Radiation Data Centre (http://wrdc.mgo.rssi.ru/wrdc_en_new.htm). * Since the data of solar radiation for Changchun (43.54° N, 125.13°E) are not available, here we present the daily solar radiation data observed for Shengyang (41.44° N, 123.31°E), which is located quite close to Changchun.

Table S2: The concentrations ($\mu g\ m^{-3}$) of organic carbon (OC), elemental carbon (EC) and inorganic ions in the filter samples of each city.

Sample ID	Sampling Date	OC	EC	Cl^-	NO_3^-	SO_4^{2-}	Na^+	NH_4^+	K^+	Mg^{2+}	Ca^{2+}
Changchun	04/01/2014	68	7.1	13.69	9.77	22.81	0.84	10.70	1.78	0.06	1.12
	24/01/2014	42	7.9	3.12	25.26	28.84	0.42	13.00	1.99	0.09	0.54
	29/01/2014	28	7.6	2.58	11.45	10.65	0.60	5.63	1.38	0.31	2.92
	Average ±*SD	46 ±20	7.5 ±0.4	6.47 ±6.26	15.49 ±8.50	20.77 ±9.27	0.62 ±0.21	9.78 ±3.78	1.72 ±0.31	0.15 ±0.13	1.53 ±1.24
Shanghai	01/01/2014	34	5.4	4.19	21.12	12.48	0.45	7.14	1.63	0.21	5.04
	19/01/2014	20	4.5	3.00	38.91	27.31	0.48	16.55	1.43	0.08	0.88
	20/01/2014	19	5.4	3.28	24.60	20.02	0.80	9.02	1.44	0.31	4.63
	Average ±SD	24 ±8	5.1 ±0.5	3.49 ±0.62	28.21 ±9.43	19.93 ±7.41	0.58 ±0.19	10.90 ±4.98	1.50 ±0.11	0.20 ±0.12	3.52 ±2.30
Guangzhou	05/01/2014	26	4.1	1.93	24.74	22.39	0.59	10.51	1.93	0.25	1.61
	06/01/2014	23	4.1	2.42	23.67	25.48	0.79	11.40	1.73	0.25	1.32
	11/01/2014	27	5.0	2.28	25.48	19.83	0.68	10.05	1.59	0.18	1.52
	Average ±SD	25 ±2	4.4 ±0.5	2.21 ±0.25	24.63 ±0.91	22.56 ±2.83	0.69 ±0.10	10.65 ±0.69	1.75 ±0.17	0.23 ±0.04	1.48 ±0.15

*SD refers to standard deviation.

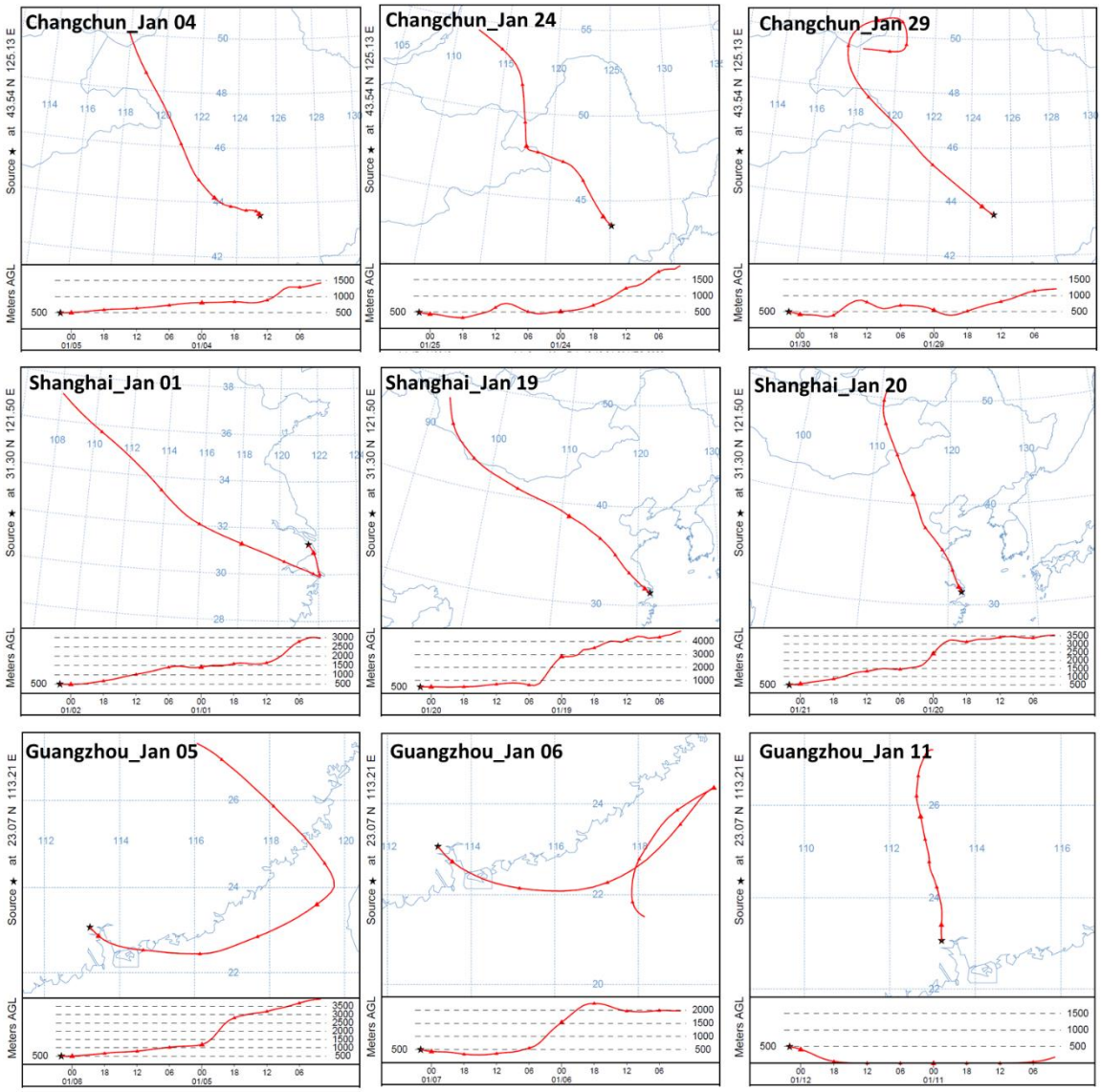

Figure S1. 48 hours back trajectories of air arriving at the three cities (Changchun, Shanghai and Guangzhou) during the sampling time calculated using the NOAA HYSPLIT model (Rolph et al., 2017).

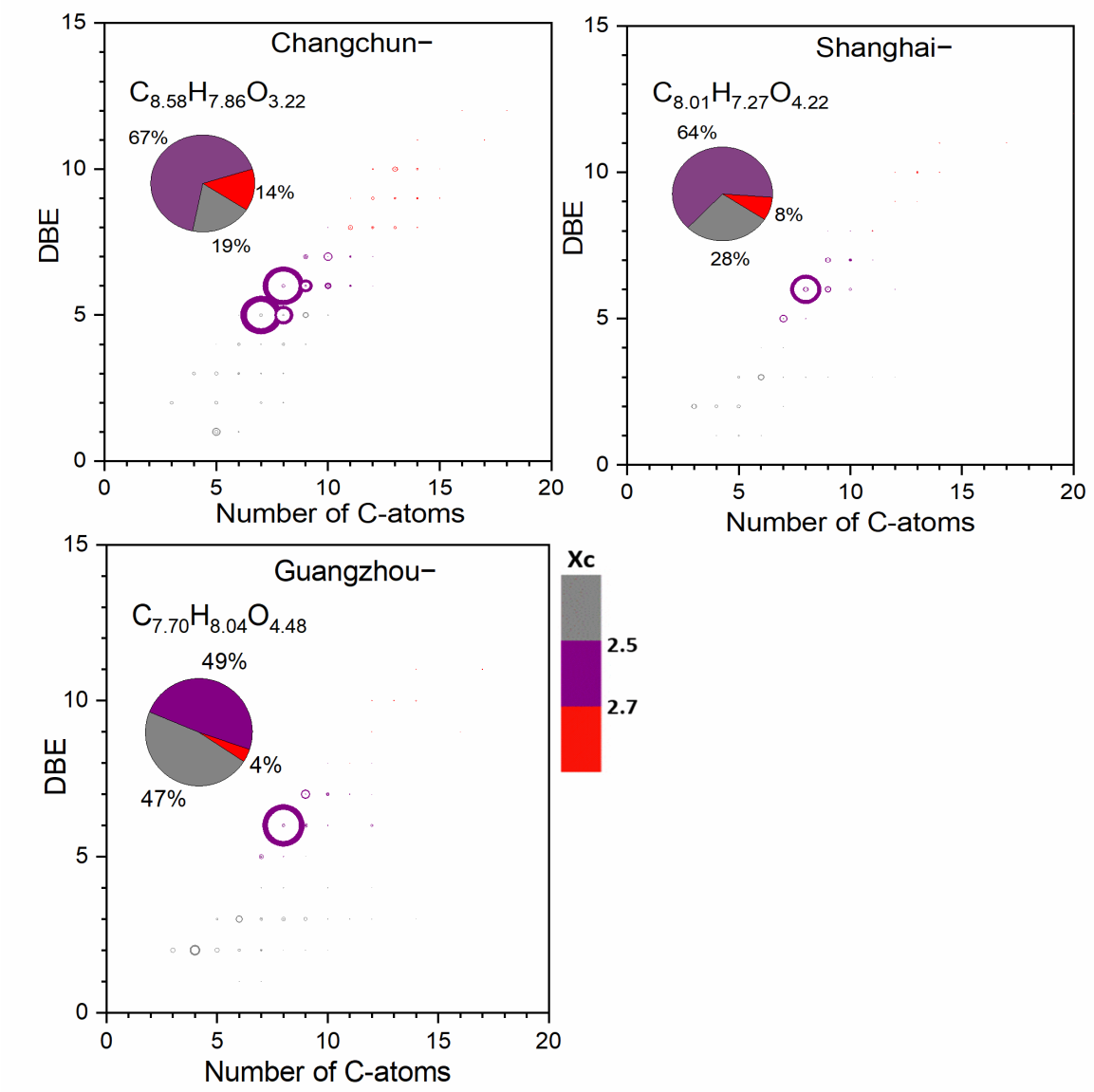

Figure S2. Double bond equivalent (DBE) versus carbon number for all CHO− compounds for all sample locations. The molecular formula represents the abundance-weighted average CHO− formula and the area of the circles is proportional to the absolute peak abundance of an individual compound. The color bar denotes the aromaticity equivalent (gray with Xc < 2.50, purple with 2.50 ≤ Xc < 2.70 and red with Xc ≥ 2.70). The pie charts show the percentage of each Xc category (i.e., gray color-coded compounds, purple color-coded compounds and red color-coded compounds) in each sample in terms of peak abundance.

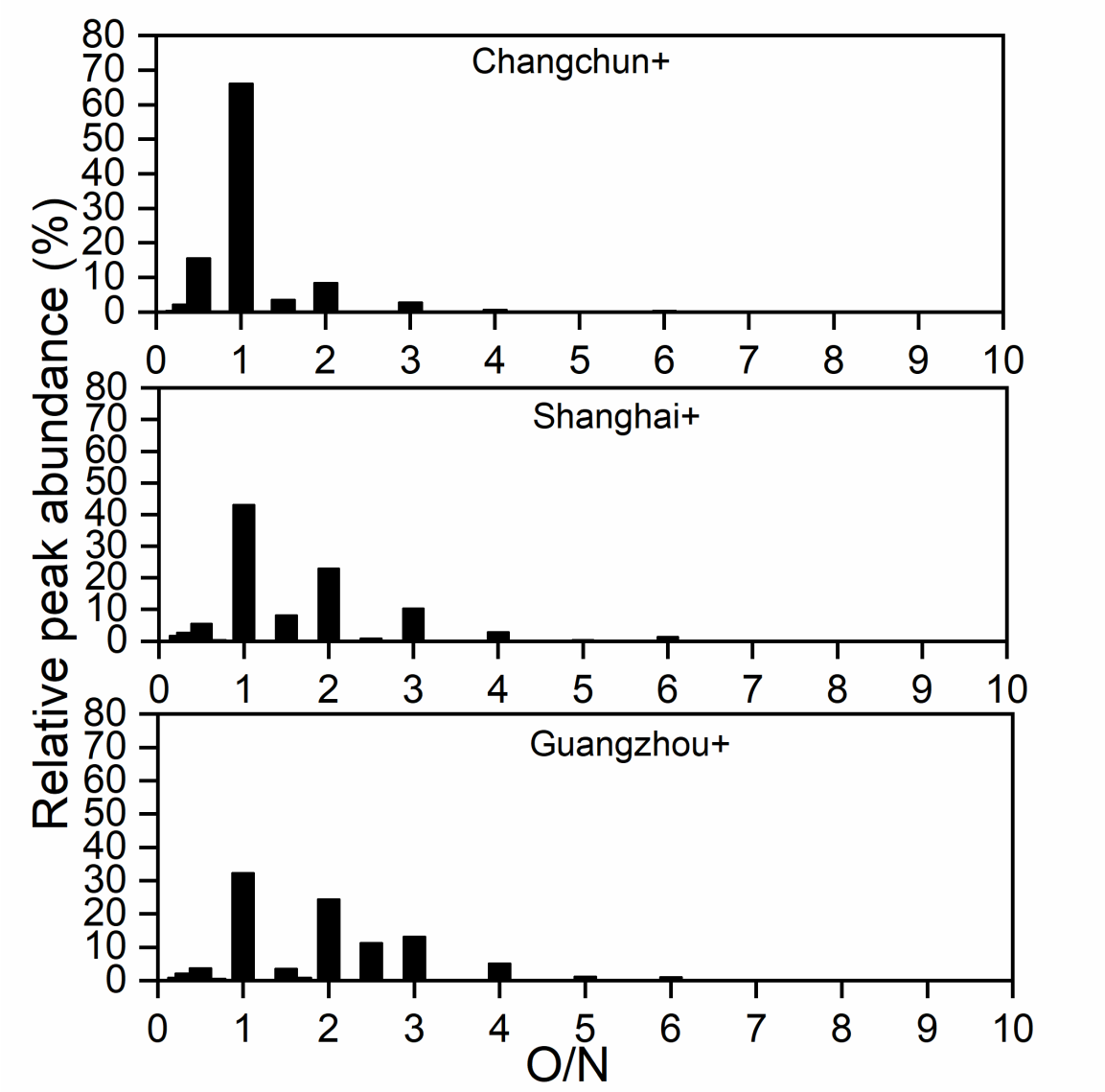

Figure S3. Classification of CHON+ compounds into different subgroups according to O/N ratios in their formulas. The y-axis indicates the relative contribution of each subgroup to the sum of peak abundance of CHON+ compounds.

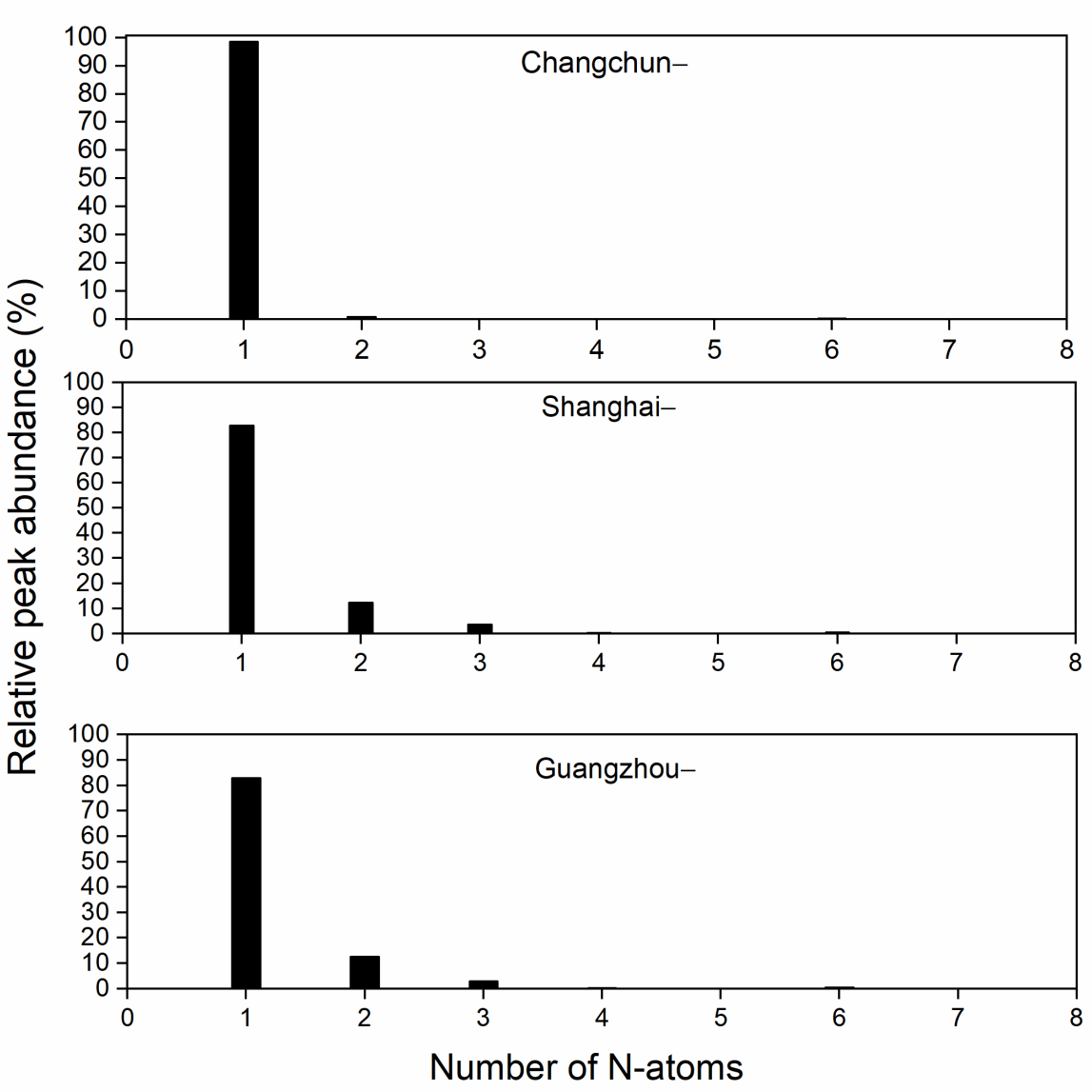

Figure S4. Classification of CHON− compounds into different subgroups according to nitrogen atoms number in their formulas. The y-axis indicates the relative contribution of each subgroup to the sum of peak abundance of all CHON− compounds.

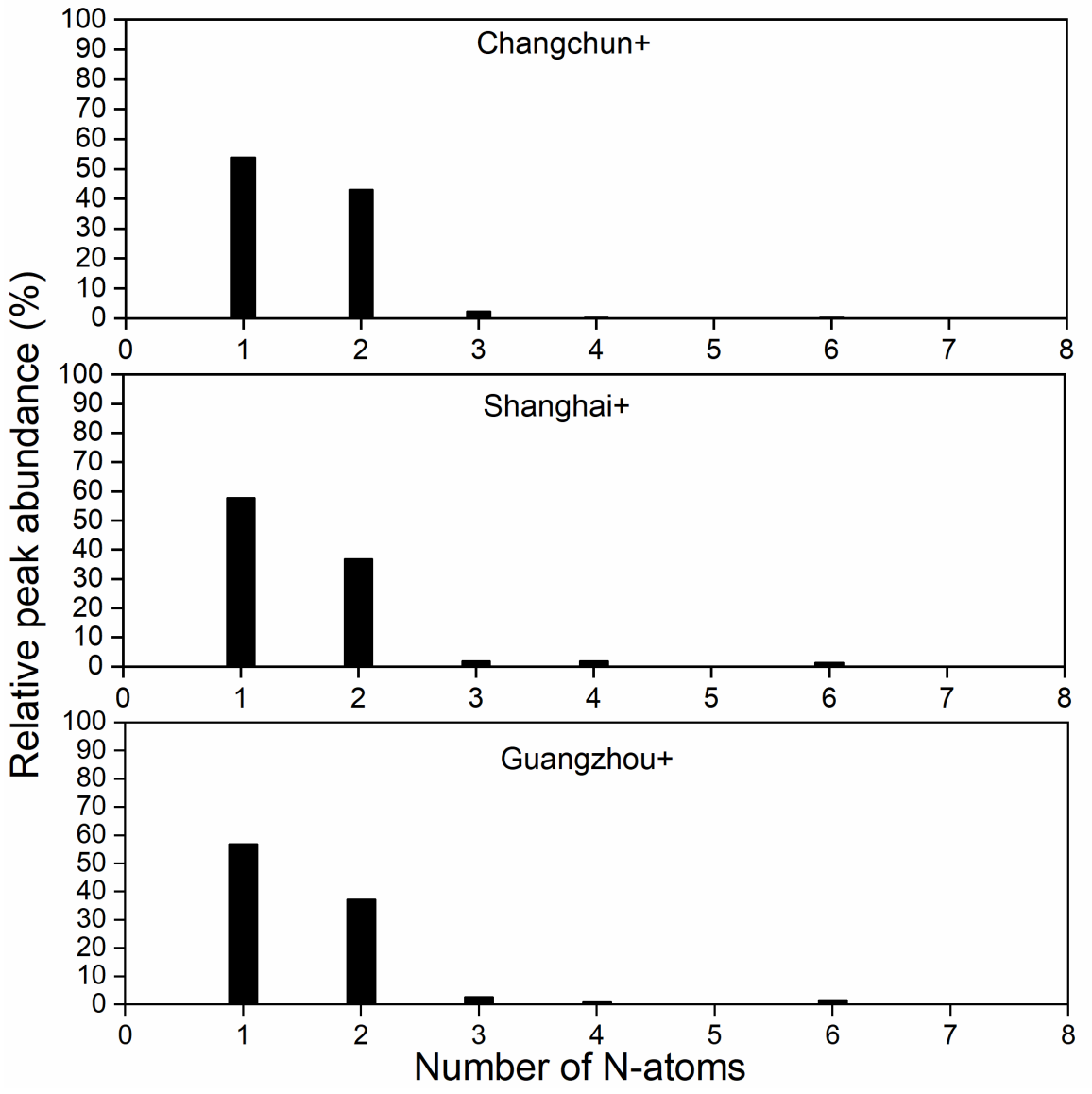

Figure S5. Classification of CHON+ compounds into different subgroups according to nitrogen atoms number in their formulas. The y-axis indicates the relative contribution of each subgroup to the sum of peak abundance of all CHON+ compounds.

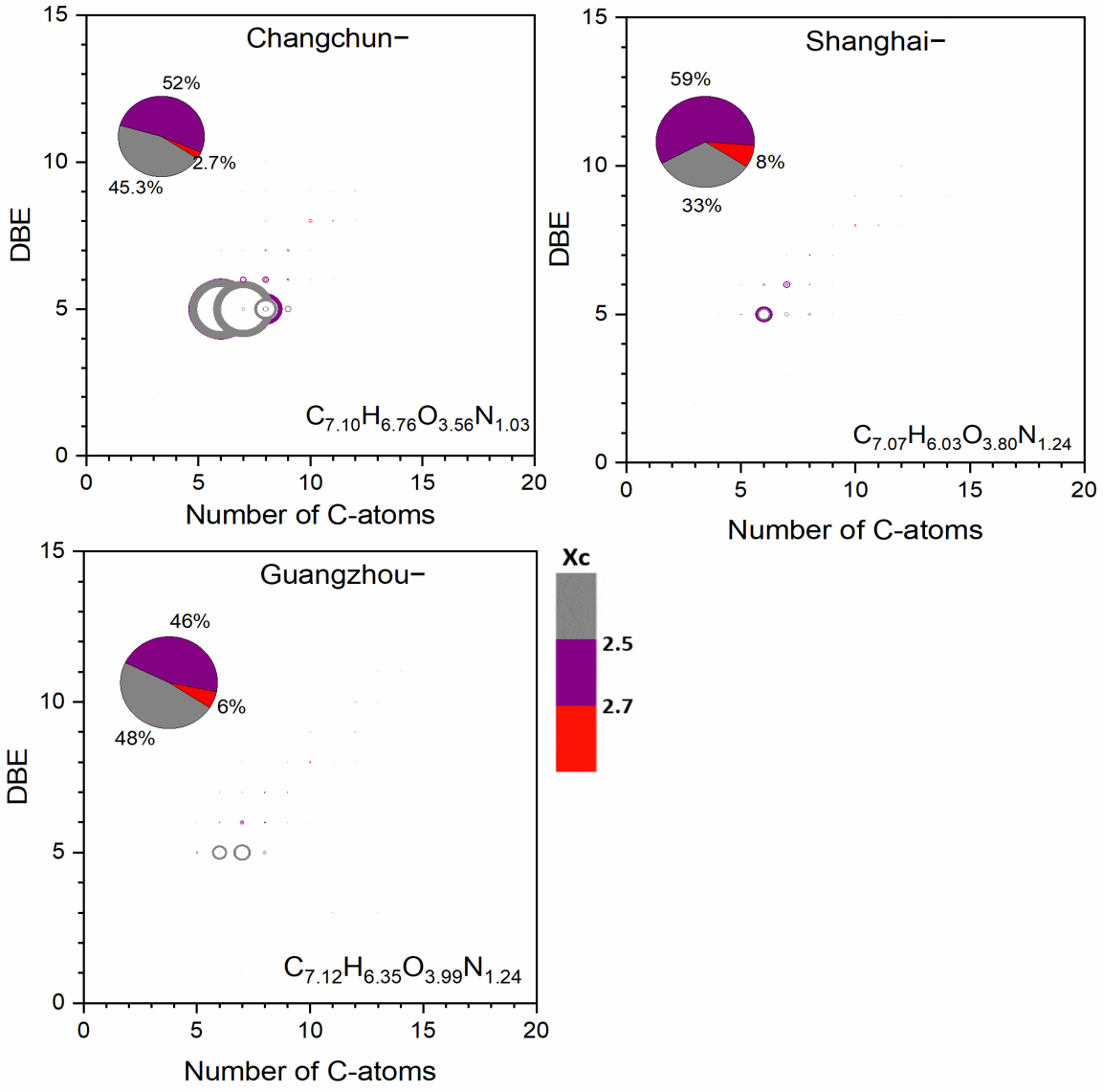

Figure S6. Double bond equivalent (DBE) versus carbon number for all CHON− compounds for all sample locations. The molecular formula represents the abundance-weighted average CHON- formula and the area of circles is proportional to the absolute peak abundance of an individual compound. The color bar denotes the aromaticity equivalent (gray with Xc < 2.50, purple with 2.50 ≤ Xc < 2.70 and red with Xc ≥ 2.70). The pie charts show the percentage of each Xc category (i.e., gray color-coded compounds, purple color-coded compounds and red color-coded compounds) in each sample in terms of peak abundance.

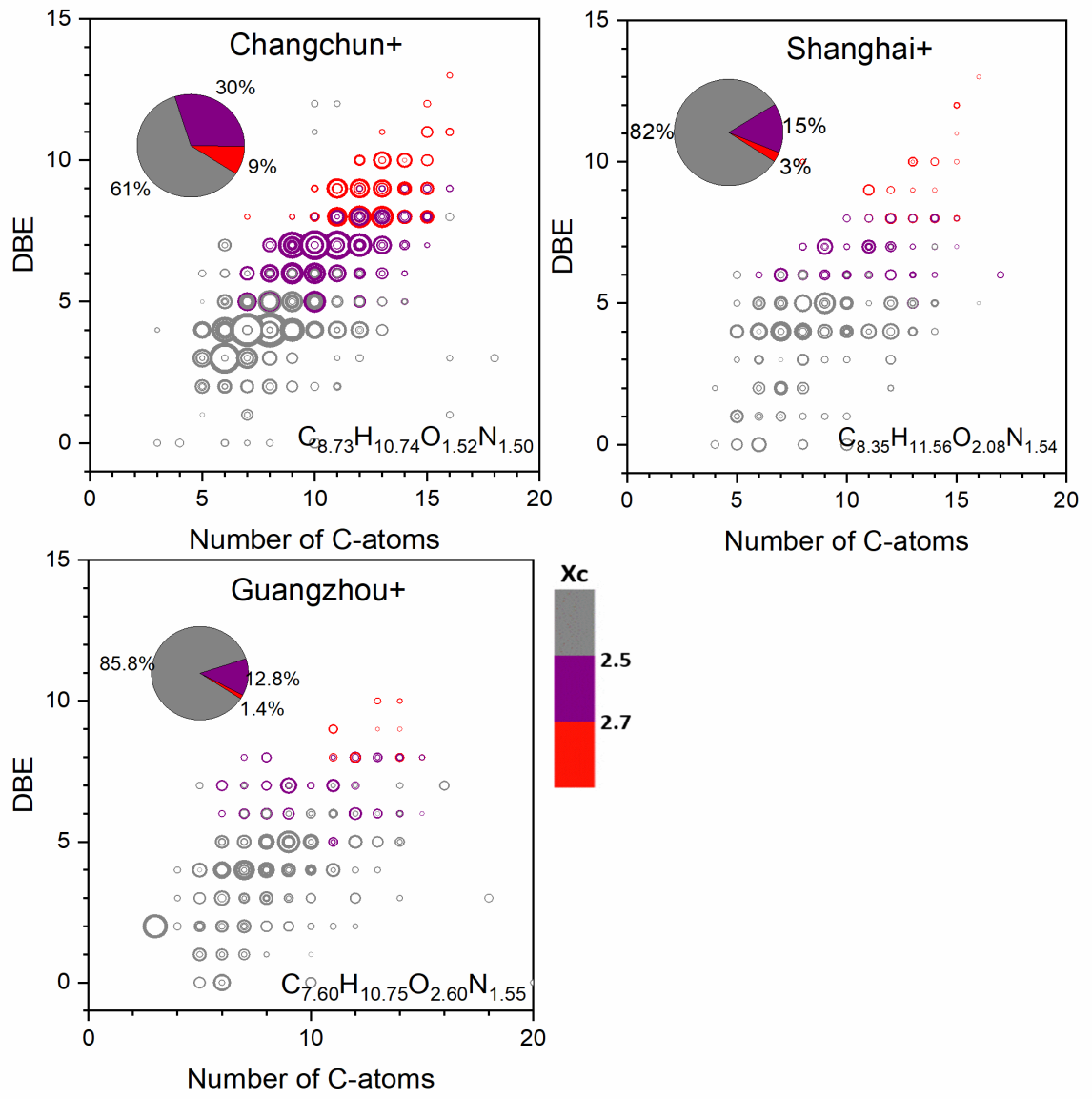

Figure S7. Double bond equivalent (DBE) vs C number for all CHON+ compounds of all samples. The molecular formula represents the abundance-weighted average CHON+ formula and the area of the circles is proportional to the fourth root of the peak abundance of an individual compound (the diagram with circle area related to absolute peak abundance is presented in Fig. S8). The color bar denotes the aromaticity equivalent (gray with Xc < 2.50, purple with 2.50 ≤ Xc < 2.70 and red with Xc ≥ 2.70). The pie charts show the percentage of each Xc category (i.e., gray color-coded compounds, purple color-coded compounds and red color-coded compounds) in each sample in terms of peak abundance.

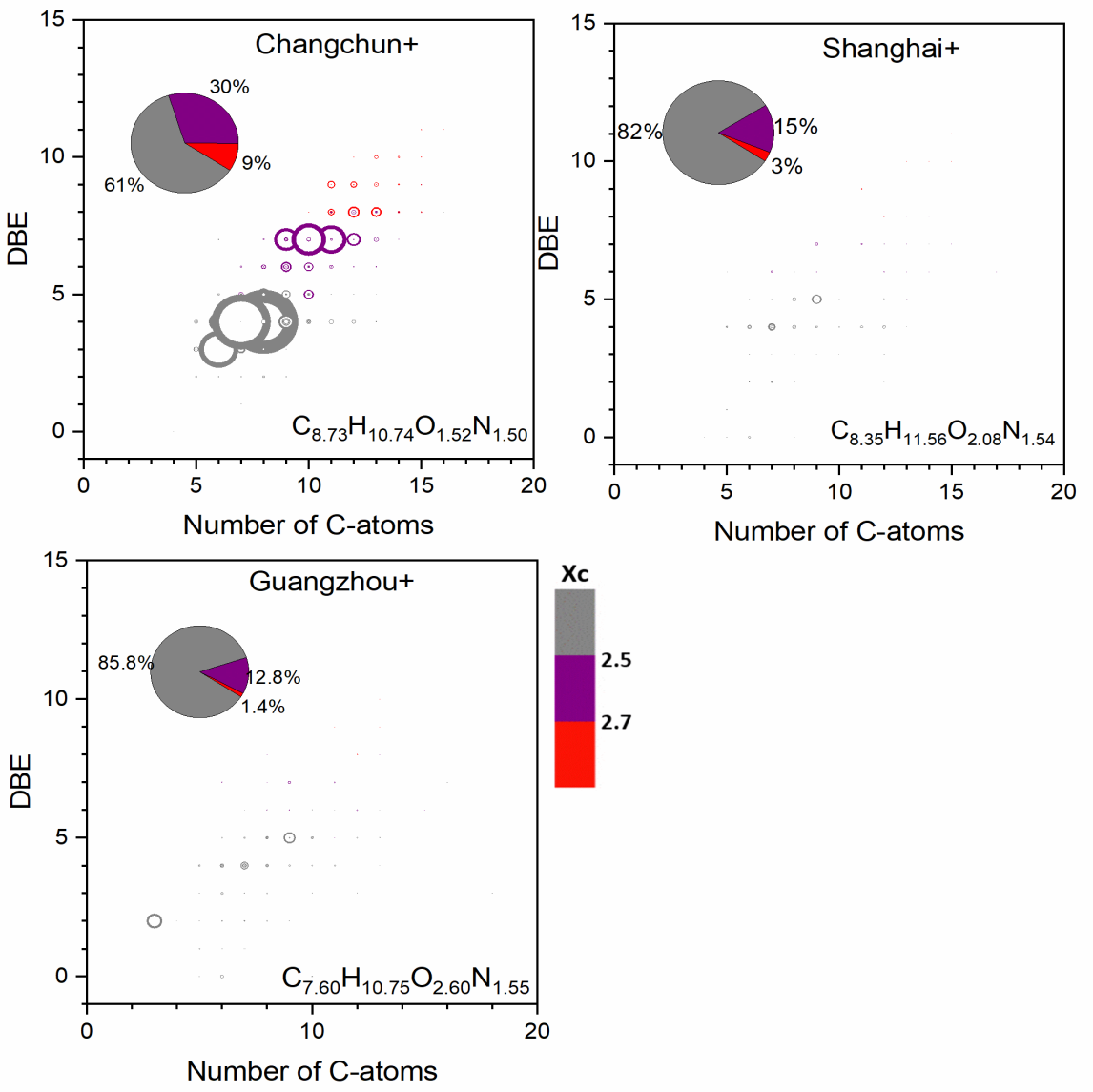

Figure S8. Double bond equivalent (DBE) vs C number for all CHON+ compounds of all samples. The molecular formula represents the abundance-weighted average CHON+ formula and the area of the circles is proportional to the absolute peak abundance of an individual compound. The color bar denotes the aromaticity equivalent (gray with Xc < 2.50, purple with 2.50 ≤ Xc < 2.70 and red with Xc ≥ 2.70). The pie charts show the percentage of each Xc category (i.e., gray color-coded compounds, purple color-coded compounds and red color-coded compounds) in each sample in terms of peak abundance.

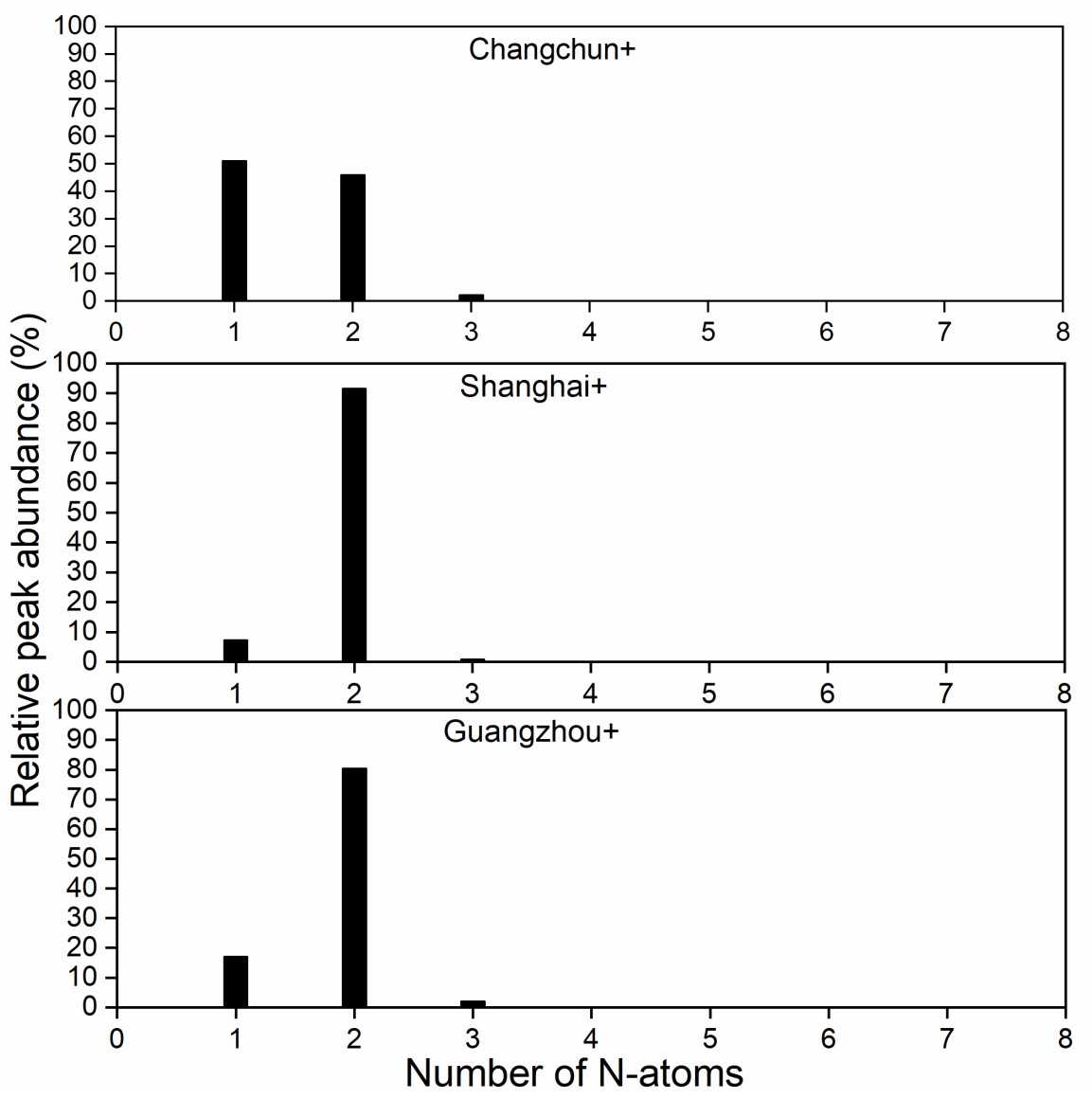

Figure S9. Classification of CHN+ compounds into different subgroups according to nitrogen atoms number in their formulas. The y-axis indicates the relative contribution of each subgroup to the sum of peak abundance of all CHN+ compounds.

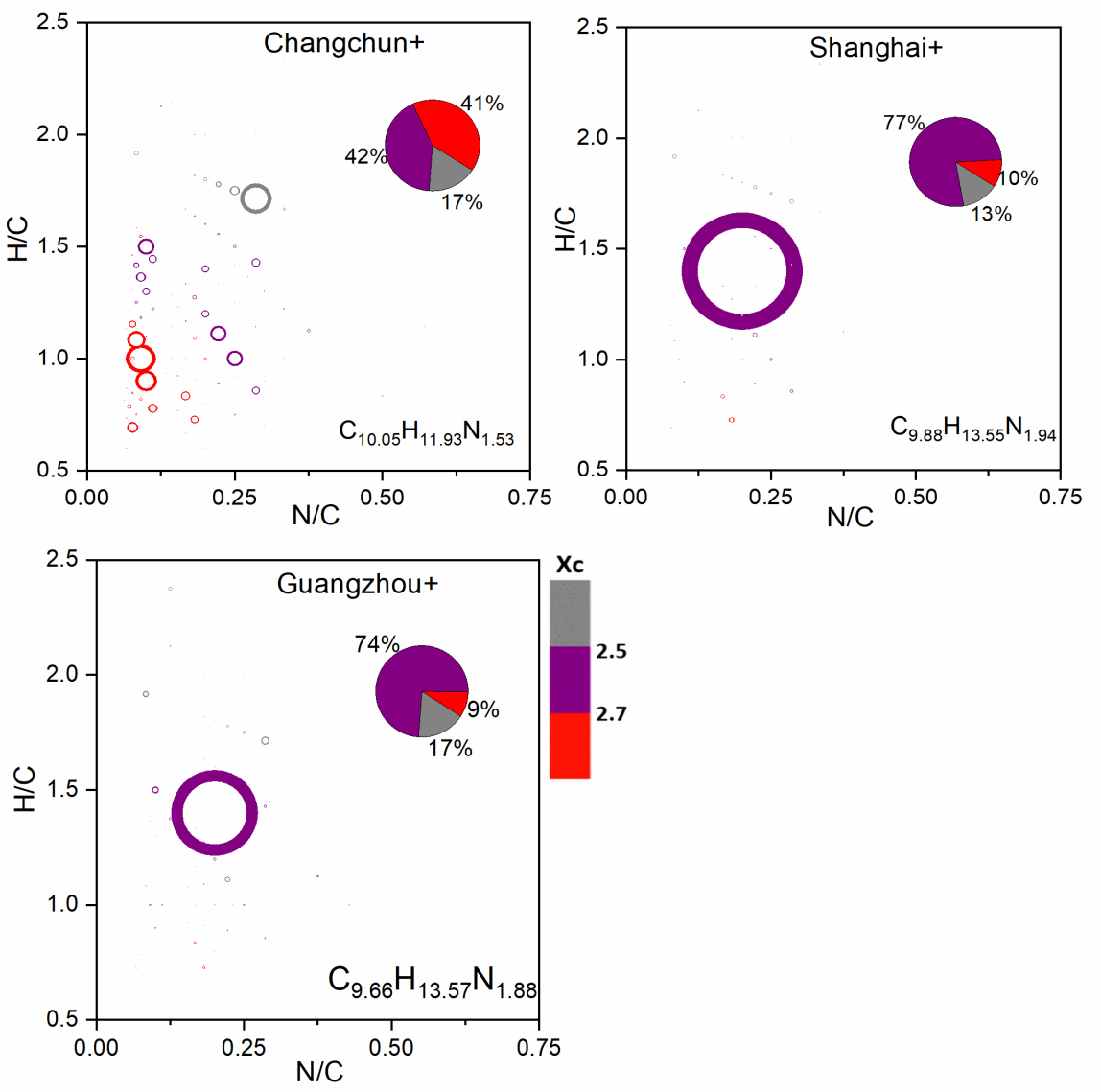

Figure S10. Van Krevelen diagrams for CHN+ compounds in Changchun, Shanghai and Guangzhou samples. The area of circles is proportional to the absolute peak abundance of an individual compound and the color bar denotes the aromaticity equivalent (gray with Xc < 2.50, purple with 2.50 ≤ Xc < 2.70 and red with Xc ≥ 2.70). The pie charts show the percentage of each Xc category (i.e., gray color-coded compounds, purple color-coded compounds and red color-coded compounds) in each sample in terms of peak abundance.

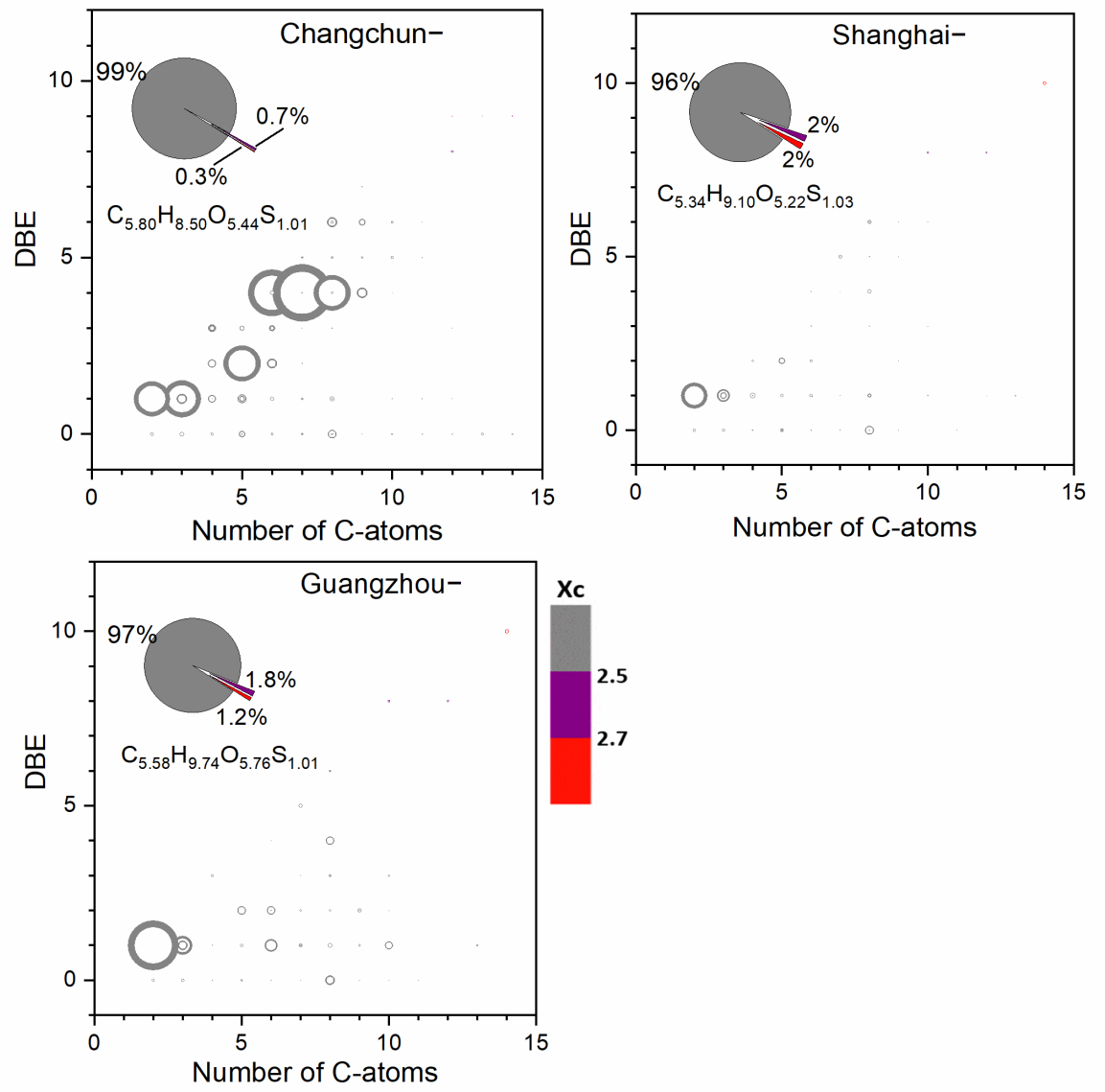

Figure S11. Double bond equivalent (DBE) versus carbon number for all CHOS− compounds for all sample locations. The molecular formula represents the abundance-weighted average CHOS− formula and the area of circles is proportional to the absolute peak abundance of an individual compound. The color bar denotes the aromaticity equivalent (gray with Xc < 2.50, purple with 2.50 ≤ Xc < 2.70 and red with Xc ≥ 2.70). The pie charts show the percentage of each Xc category (i.e., gray color-coded compounds, purple color-coded compounds and red color-coded compounds) in each sample in terms of peak abundance.

References

Kind, T., and Fiehn, O.: Seven Golden Rules for heuristic filtering of molecular formulas obtained by accurate mass spectrometry, BMC Bioinformatics, 8, 10.1186/1471-2105-8-105, 2007.

Kourtchev, I., Godoi, R. H. M., Connors, S., Levine, J. G., Archibald, A. T., Godoi, A. F. L., Paralovo, S. L., Barbosa, C. G. G., Souza, R. A. F., Manzi, A. O., Seco, R., Sjostedt, S., Park, J.-H., Guenther, A., Kim, S., Smith, J., Martin, S. T., and Kalberer, M.: Molecular composition of organic aerosols in central Amazonia: an ultra-high-resolution mass spectrometry study, Atmos. Chem. Phys., 16, 11899-11913, https://doi.org/10.5194/acp-16-11899-2016, 2016.

Lin, P., Rincon, A. G., Kalberer, M., and Yu, J. Z.: Elemental composition of HULIS in the Pearl River Delta Region, China: results inferred from positive and negative electrospray high resolution mass spectrometric data, Environ. Sci. Technol., 46, 7454-7462, 10.1021/es300285d, 2012.

Rincón, A. G., Calvo, A. I., Dietzel, M., and Kalberer, M.: Seasonal differences of urban organic aerosol composition - an ultra-high resolution mass spectrometry study, Environ. Chem., 9, 298, 10.1071/en12016, 2012.

Rolph, G., Stein, A., and Stunder, B.: Real-time Environmental Applications and Display sYstem: READY, Environ. Model. Softw., 95, 210-228, 10.1016/j.envsoft.2017.06.025, 2017.

Wang, K., Zhang, Y., Huang, R.-J., Cao, J., and Hoffmann, T.: UHPLC-Orbitrap mass spectrometric characterization of organic aerosol from a central European city (Mainz, Germany) and a Chinese megacity (Beijing), Atmos. Environ., 189, 22-29, 10.1016/j.atmosenv.2018.06.036, 2018.

Wang, X. K., Hayeck, N., Brüggemann, M., Yao, L., Chen, H. F., Zhang, C., Emmelin, C., Chen, J. M., George, C., and Wang, L.: Chemical characterization of organic aerosol in: A study by Ultrahigh-Performance Liquid Chromatography Coupled with Orbitrap Mass Spectrometry, J. Geophy. Res.-Atmos., 122, 703-722, https://doi.org/10.1002/2017JD026930, 2017.

Yassine, M. M., Harir, M., Dabek-Zlotorzynska, E., and Schmitt-Kopplin, P.: Structural characterization of organic aerosol using Fourier transform ion cyclotron resonance mass spectrometry: aromaticity equivalent approach, Rapid Commun. Mass Spectrom., 28, 2445-2454, 10.1002/rcm.7038, 2014.

Zielinski, A. T., Kourtchev, I., Bortolini, C., Fuller, S. J., Giorio, C., Popoola, O. A. M., Bogialli, S., Tapparo, A., Jones, R. L., and Kalberer, M.: A new processing scheme for ultra-high resolution direct infusion mass spectrometry data, Atmos. Environ., 178, 129-139, 10.1016/j.atmosenv.2018.01.034, 2018.